HHS Public Access

Author manuscript

Neuroimage. Author manuscript; available in PMC 2016 July 15.

Published in final edited form as:

Neuroimage. 2015 July 15; 115: 30–41. doi:10.1016/j.neuroimage.2015.04.043.

3D Cortical Electrophysiology of Ballistic Upper Limb Movement in Humans

Edward Ofori, PhD[1], **Stephen A. Coombes, PhD**[1], and **David E. Vaillancourt, PhD**[1,2,3]

[1]Department of Applied Physiology and Kinesiology, University of Florida, Gainesville, FL 32611

[2]Department of Biomedical Engineering, University of Florida, Gainesville, FL 32611

[3]Department of Neurology, University of Florida, Gainesville, FL 32611

Abstract

Precise motor control requires the ability to scale the parameters of movement. Theta oscillations across the cortex have been associated with changes in memory, attention, and sensorimotor processing. What has proven more elusive is pinpointing the region-specific frequency band oscillations that are associated with specific parameters of movement during the acceleration and deceleration phases. We report a study using 3D analytic techniques for high density electroencephalography that examines electrocortical dynamics while participants produce upper limb movements to different distances at varying rates. During fast ballistic movements, we observed increased theta band activity in the left motor area contralateral to the moving limb during the acceleration phase of the movement, and theta power correlated with the acceleration of movement. In contrast, beta band activity scaled with the type of movement during the deceleration phase near the end of the movement and correlated with movement time. In the ipsilateral motor and somatosensory area, alpha band activity decreased with the type of movement near the end of the movement, and gamma band activity in visual cortex increased with the type of movement near the end of the movement. Our results suggest that humans use distinct lateralized cortical activity for distance and speed dependent arm movements. We provide new evidence that a temporary increase in theta band power relates to movement acceleration and is important during movement execution. Further, the theta power increase is coupled with desychronization of beta and alpha band power which are modulated by the task near the end of movement.

Keywords

ICA; Theta band oscillations; Motor cortex; Beta band dysnchronization; MPA

Corresponding Author: David E. Vaillancourt, PhD, Department of Applied Physiology and Kinesiology, University of Florida, PO Box 118205, (e) vcourt@ufl.edu (o) 352-294-1770, (f) 352-392-5262.

1. Introduction

Visually-guided ballistic movement tasks involve activation and synchrony of multiple cortical regions and specific muscles to move the limb from point A to point B. Consider a tennis drop shot from superstar Serena Williams. She must locate the ball in space and time, accelerate her upper arm with the racket towards the ball, make contact with the ball, and then decelerate the movement of the upper arm. Such a ballistic movement requires an initial agonist burst of upper arm flexor muscles and a delayed antagonist burst of opposing muscles. Importantly, racket motion has to be scaled depending on the goal of the movement. The goal in the current study is to determine the timing and oscillatory nature of the cortical activity in specific brain regions that are involved in the control of visually guided ballistic arm movements.

Oscillations of cortical activity at specific frequencies may reflect different functions such as movement anticipation (McFarland et al., 2000) and visual information processing (Cruikshank et al., 2012). In sensorimotor tasks, prior studies have examined alpha and beta band oscillations from specific electrodes and found event-related desynchronization at the beginning of movement (Allen and MacKinnon 2010; Kilavik et al., 2013; Pfurtscheller and Neuper 1994). In addition to alpha and beta, classic animal studies over two decades ago led Bland (1986) to suggest that theta band activity facilitates information processing and several authors have since extended this hypothesis to humans (Cruikshank et al., 2012; Kahana et al., 1999). For instance, event-related desynchronization of beta coincides with increased synchronization of theta band activity at movement initiation and during the beginning of movement (Cruikshank et al., 2012). However, it is not clear whether these oscillations are sensitive to the specific parameters of movement. Since theta band activity has been shown to increase at the beginning of movement and prior studies in non-human primates have shown that single cells in layer 5 of the motor cortex are predictors of specific movement parameters (Ashe and Georgopoulos 1994), we tested the hypothesis that theta band power in the contralateral motor cortex of humans would increase at the beginning of movement. The main goal in the current study was to determine which parameters of movement related most closely to theta band activity.

Time-frequency analyses in electrode space have traditionally been used to infer cortical or subcortical activity. This approach has created some ambiguity for the localization of event-related synchronization and desynchronization in sensorimotor areas (Jurkiewicz et al., 2006; McFarland et al., 2000; Salmelin and Hari 1994). One novel approach that can provide more accurate cortical localization is to apply independent component analysis (ICA) of EEG (Delorme and Makeig 2004) and measure projection analysis (MPA) of ICA signals. The combination of these analytic methods allows high-density electroencephalography (EEG) to be treated and used as a three-dimensional functional imaging modality (Bigdely-Shamlo et al., 2013). In the current study, ICA and MPA were used on high-density EEG source signals to examine electrocortical dynamics while participants produced upper limb movements to different distances at varying speeds. Here we determine how theta band activity in the contralateral motor region is associated with movement kinematics during the beginning of movement. We also detail changes in alpha,

beta, and gamma band activity across other cortical domains at different time points of the movement.

2. Materials and Methods

2.1 Subjects

Fifteen participants (mean age: 25.7±5.5 yrs.; 9 females) were recruited for this study. All participants were self-reported healthy right-handed individuals with normal or corrected vision. Participants were asked to refrain from consuming caffeine and using any hair products on the day of testing. Prior to experimental testing, participants provided informed consent. This experimental study was approved by the local Institutional Review Board.

2.2 Experimental Design and Task

The experimental setup was similar to prior work (Vaillancourt et al., 2004). Each participant sat upright in a chair with his or her right arm supported against a cantilever beam attached to a custom-made manipulandum. The beam was attached to an angle transducer (Trans-Teck., Ellington, CT). The beam was located 70 cm above ground and could move 110 degrees in the transverse plane. Figure 1A shows a participant's body configuration at the beginning and end of a trial. During each trial, the participant viewed a computer monitor that displayed a start position, a target location, and a cursor whose position is controlled by the participant's arm displacement. Figure 1A also shows the visual display from the computer monitor of the short and long conditions at the beginning and end of the desired movement. A yellow cross-haired cursor indicated angular position to the participant, a white rectangular box indicated the start position, and a green rectangular box indicated the target location.

The green target box was presented on the screen at one of 2 locations (12° or 72°) relative to the start position. The green target box spanned a ±1.25° horizontal area of the desired target location. Each participant was required to flex his or her elbow horizontally from the start position to the target location. Each participant performed 3 conditions: 1) to move "as fast and accurately as possible" to a 12° target (Short), 2) to move "as fast and accurately as possible" to a 72° target (LongF), and 3) to move "as comfortably and accurately as possible" to the 72° target (LongC). These conditions were chosen to determine how movement parameters change with electrocortical activity in the cortex. Significant findings that were common to all contrasts would provide a robust measure of the cortical oscillations that are associated with various movement parameters. All participants performed 60 trials at each condition (10 practice, and 50 experimental trials) in a blocked paradigm. The block order was randomized across all participants.

For all blocks the same series of events occurred. The visual display shown in Figure 1A was displayed for 12 seconds and disappeared between trials. There were three total auditory beeps for one trial. The first beep was the preparatory beep and this cued the subject to get ready for the task. The second beep was the go beep which cued movement to begin and this came 3s after the preparatory beep. The third beep was the end beep and came 4s after the go beep and this cued the subjects to move their limb back to the start position for the next

trial. Subjects moved their limb back to the start position at a comfortable pace. The trial ended 5s after the end beep and the visual display disappeared. The computer then saved the data for about 1–2s, and then the next trial commenced such that the visual display came on, and the first preparatory beep occurred.

2.3. Data Acquisition

The MotionMonitor (Innovative Sports Training, Inc, Chicago, IL) system was configured to synchronize data in real time from EMG, EEG, and kinematic systems using an analogue sync pulse.

2.3.1. Kinematic data acquisition—The kinematic data were collected with an angular displacement transducer. The transducer was mounted at the axis of rotation of the manipulandum. An excitation voltage of 16 V from a Leader LPS-152 DC Tracking Power Supply (Advanced Test Equipment Rentals, San Diego, CA) was used to power the angular displacement transducer. The displacement data were transmitted via a 16-bit A/D converter and digitized at 1000 Hz using a USB-1616HS-BNC A/D board (Measurement Computing, Norton, MA).

2.3.2. EMG data acquisition—EMG data were collected with the Delsys Trigno Wireless System (Delsys Inc, Boston, MA). Participants were prepped by rubbing the desired locations on the right arm with alcohol. Two channels were used to measure electrophysiological activity from the muscle. The wireless EMG electrodes were placed at two locations on the participant's right arm. The two locations were the biceps brachii and triceps lateral head. The EMG data were sampled at 1000 Hz.

2.3.3. EEG data acquisition—EEG data were collected with the ActiveTwo system that was comprised of 128 Ag-AgCl Active Two electrodes. The active electrodes were connected to a cap that was in a preconfigured montage covering the entire scalp. One of three cap sizes was selected based on the participant's head circumference (i.e., 50–54 cm, 54–58 cm, or 58–62 cm). The signals were amplified through the electrodes at the source and had an output impedance of <1 ohm. EEG signals were digitally amplified at DC and sampled at 2,048 Hz. Electrical potentials were recorded between each electrode and the common mode sense (CMS) electrode. The CMS and the driven right leg (DRL) electrode were located at the center of the scalp in relation to all other electrodes. The CMS and DRL electrodes were used to drive the average potential of the subject as close as possible to the AD-box reference potential electrode. The electrode offsets, a running average of the voltage measured between the CMS and each active electrode, were evaluated before the start of each condition and during data collection to be within the acceptable range of 40 μV. The electrode offset served as an indirect measure of impedance tolerance. To ensure that a stable and high quality signal was recorded from each active electrode throughout the recording session, the electrode offset was monitored. Motion monitor synced all EEG, EMG, and kinematic signals into one data file using the sync pulse that was collected during data acquisition for each trial.

2.4. Data Processing and Analysis for EEG Event-related Spectral Perturbation

All behavioral and electrophysiological data were imported into MATLAB 2011 (The Mathworks, Natick, MA). Angular position data were lowpass filtered at 30 Hz (Butterworth 4th order dual pass). Velocity and acceleration were obtained by differentiating the angular position signal. The beginning of movement was determined from acceleration data. This was accomplished by searching backward from peak acceleration until an acceleration data sample was 5% of peak acceleration and the end of the movement was determined by searching forward from peak deceleration and finding the first point that was 5% of peak deceleration. Final displacement, peak velocity, peak acceleration, peak deceleration, peak error, and movement time were computed from the kinematic data. Peak error was computed as the final displacement minus the required target distance. The final displacement was computed at the first zero crossing of the velocity trace after the beginning of movement. A 1-way repeated measures ANOVA was conducted on the Short, LongF, and LongC conditions. Significant main effects were followed up with pairwise comparisons with Bonferroni correction between conditions and Bonferroni corrected p-values are reported. Peak acceleration and peak velocity were the main variables of interest during the beginning of movement and peak deceleration, peak error, final displacement, and movement time were the main variables at the end of the movement.

2.4.1. EMG Analysis—EMG data were highpass filtered at 1 Hz (Butterworth 5th order dual pass) to remove the DC offset, rectified, and then lowpass filtered at 50 Hz (Butterworth 5th order dual pass). Integrated EMG (iEMG) was computed across four phases of movement from movement onset to peak acceleration, peak acceleration to peak velocity, peak velocity to peak deceleration, and peak deceleration to the end of movement. A 4 (phase) x 3 (task condition) repeated measures ANOVA was conducted for each muscle. If the interaction for each muscle was significant, a repeated measures ANOVA with the factor task condition was performed at each of the 4 phases of the movement to determine how muscle activity changed within each condition at each phase.

2.4.2. EEG Analysis Step 1—EEG data were processed using custom scripts based on EEGLAB, an open source Matlab toolbox for processing electrophysiological data (Delorme and Makeig 2004). First, the EEG channels with a standard deviation larger than 1000 μV were interpolated. This interpolation procedure weighted the remaining channels as a function of their corresponding distance from the channel to be reconstructed. On average, seven channels were interpolated (range: 0–18; standard deviation: 5.3). EEG data were bandpass filtered between 1 and 70 Hz. The data were then re-referenced to a common average reference. One second epochs of EEG data were extracted before the beginning of movement and then EEG data were time normalized from the beginning to the end of movement for all trials (Gwin et al., 2010). This normalization procedure involved using EEGLAB scripts that selected epochs from all individuals and time warping these epochs to a common timebase. We then used the first half of the common time base to indicate the beginning of movement and the second half of the time base to indicate the end of movement. The data were manually inspected for eye blinks and eye movements and trials were rejected based on occurrence. Epochs were rejected from further analysis with a probability occurrence > 3 SD and kurtosis ≥ 5 from the mean across all trials (Gwin and

Ferris 2012). Ten trials (17%) per condition on average were removed from further analysis. The remaining data were decomposed using independent component analysis (ICA).

2.4.3. EEG Analysis Step 2—Infomax ICA using EEGLAB routines decomposed the data into independent components for each individual. The “runica” Infomax algorithm was used to detect supergaussian and subgaussian sources of activity. The ICA weights and sphering matrices were multiplied by the data to form independent components (ICs). DIPFIT functions within EEGLAB were used to compute an equivalent current dipole model that best explained the scalp topography of each independent component. Each dipole was identified through a finite element spherical head model from Brain Electrical Source Analysis [BESA (BESA GmbH, Gräfelfing, GE)]. The digitized electrode locations were aligned with the head model by scaling the coordinate system so that the reference points of the scalp model matched the anatomical reference points of the spherical head model. These coordinates were converted to normalized Montreal Neurological Institute (MNI) space. Independent components were excluded if the projection of the equivalent current dipole to the scalp accounted for more than 20% of the residual variance, outside of the brain, or if the time-course, spectra, and topography of ICs were reflective of eye movement or electromyography artifact.

2.4.4. EEG Analysis Step 3—Measure projection analysis (MPA) was applied to the EEG data using a Measure Projection Toolbox for MATLAB operating as an EEGLAB plug-in (Bigdely-Shamlo et al., 2013). MPA identifies domains that include the individual subject ICs. The standard deviation of the three-dimensional Gaussian representing each dipole location distribution was set to 12 mm. Each Gaussian that represented a dipole was truncated to a radius of 3 standard deviations (36 mm) to prevent influences from distant dipoles. To define anatomical regions of interest (ROIs) and find ratios of domain masses for cortical structures, the toolbox incorporates the probabilistic atlas of human cortical structures provided by the LONI project (Shattuck et al., 2008).

A cubic dipole space grid with 8-mm spacing was situated in the brain volume in MNI space and served as the MPA brain model. Voxels outside the brain model were excluded. Local convergence values were calculated based on the algorithm explained in detail by Bigdely and colleagues (2013). Local convergence helps deal with the multiple comparisons problem by finding measure similarity of dipoles and comparing them with randomized dipoles. A pairwise IC similarity matrix was constructed by estimating the signed mutual information between independent component-pair event-related power spectral perturbation (ERSP) and inter-trial coherence (ITC) measure vectors using a Gaussian distribution assumption. Signed mutual information was estimated to improve the spatial smoothness of obtained MPA significance values (Bigdely-Shamlo et al., 2013). A significance threshold for convergence at each brain location was obtained by bootstrap statistics. The raw voxel significance threshold was set to $p<0.01$. Voxels with convergence probabilities lower than this threshold defined the measure convergence substance of voxel locations at which the local similarity of independent component ERSPs and ITCs was significantly higher. This analysis provides the cortical domains that represent independent components.

2.4.5. EEG Analysis Step 4—Within each domain, ERSPs and ITCs were computed for each condition to identify region-specific and frequency-specific oscillatory activity during the movement. Theta oscillations were from 4–8 Hz, alpha was from 8–12 Hz, beta was from 13–30 Hz, and gamma was from 35–50 Hz. For each identified domain, significant differences in the power at each frequency between Short, LongF, and LongC were computed by first projecting the ERSP associated with each condition to each voxel in a domain. This produced a projected measure. Next, a weighted-mean measure across all domain voxels was weighted by the dipole density of an individual voxel per participant. The measure was then normalized by the total domain voxel density. Next, separate bootstrapped two-tailed student-T tests were applied to make comparisons across conditions. Bootstrapped t-tests were used to control the type I error rate. Analysis of projected source measures were separated into distinct spatial domains by threshold-based Affinity Propagation clustering based on a similarity matrix of pair-wise correlations between ERSP and ITC measure values for each position. For the current study, the maximal exemplar-pair similarity, a parameter that ranges from 0 – 1.0 was set to a value of 0.8 based on prior work (Bigdely-Shamlo et al., 2013). A high domain exemplar creates more domains at smaller spatial sizes, whereas a small domain exemplar creates larger spatial domain sizes from the given data. As such, domains may contain subcortical and cortical areas due the exemplar chosen in this study.

2.5. Correlation Analysis between ERSP Power and Movement Kinematics

We examined the relation between mean power in the ERSP with movement kinematics. Following the statistical analysis that identified specific points in time when the ERSP differed consistently across conditions, the correlation coefficient and associated t statistic were computed for each kinematic parameter including peak acceleration, peak deceleration, peak velocity, movement time, and movement error. In the correlation, the average kinematic parameter across all trials per condition for each subject was included, indicating 45 data points in the correlation analysis. To control for multiple comparisons, a correction at a false discovery rate (FDR) of .05 was performed using the Benjamini-Hochberg-Yekutieli method in MATLAB. The method can be found at: http://www.mathworks.com/matlabcentral/fileexchange/27418-benjamini-hochbergyekutieli-procedure-for-controlling-false-discovery-rate/content/fdr_bh.m. The FDR adjusted p-values are reported.

3. Results

3.1. Behavior and Electromyography

Figure 1B and 1C and Table 1 show peak acceleration, peak velocity, peak deceleration, movement time, peak error, and distance values for each condition. Significant effects for task condition were found on all the behavioral data (see Table 1). Post hoc results found that the LongF condition had greater mean values for all dependent measures shown in Table 1 and Figure 1. Short and LongC had peak acceleration and peak error that did not differ. As expected, the Short condition also had shorter distance and less movement time compared with the LongC and LongF conditions.

Figure 1D and Tables 2A and 2B show the integrated EMG (iEMG) values over four phases of the movement for the biceps brachii and triceps lateral across conditions. The four phases were the beginning of movement to peak acceleration, peak acceleration to peak velocity, peak velocity to peak deceleration, and deceleration to the end of movement. Significant effects for condition were found during all phases of movement for the biceps brachii and the latter phases (i.e., three and four) of movement for the triceps lateral (see Figure 1D and Tables 2A and 2B). Post hoc results for the biceps found greater iEMG for the LongF condition than the LongC and Short condition during phases 1 and 4. Phases 2 and 3 for the biceps resulted in greater iEMG in the LongC than the Short condition. LongF and LongC iEMG for biceps were not significantly different during phase 2, whereas LongC was greater than Short for phase 3. Post hoc results for the triceps found greater iEMG in the LongC condition than the LongF and Short conditions during phase 3. For the last phase of the movement, results indicated greater iEMG in the LongF and Short conditions when compared with the LongC condition.

3.2. Source-Space Cortical Dynamics: Event-related Spectral Pertubations

Figures 2–5 show ERSP measure cortical domains, their respective time-frequency plots and statistical significance plots from all experimental conditions. One hundred-six ICs from EEG signals contributed to the left motor area, 92 ICs for the right motor area, 62 ICs for the somatosensory area, and 55 ICs for the right/visual area. Each subject contributed at least 2 ICs to each of the ERSP domains for 315 electrical sources. The locations and nomenclature for this study are based on the Laboratory of NeuroImaging (LONI) project probabilistic atlas (Shattuck et al., 2008) and the corresponding Brodmann areas are shown in Table 3. Paired t-tests were conducted on ERSP from each ERSP domain. EEG analyses focused on data from the beginning of movement to the end of movement. We examined ERSP comparisons to determine if the data were consistent with kinematic parameters at the beginning and end of movement (see Figure 1B and 1C).

Figure 2A shows a left motor area that is consistent with primary, premotor, and supplementary motor cortex (BA 4 and 6) and primary somatosensory cortex (BA 3). Figure 2B shows the time-frequency spectral plots from ERSP Domain 1 for each condition. Figure 2C shows the statistical comparison of time-frequency plots for the LongF vs. Short, LongF vs. LongC, and LongC vs. Short conditions. Statistical analysis revealed the LongF condition had greater spectral power in the theta band than the Short condition and the LongC condition at the beginning of the movement [$t(14)'s \geq 3.34, p's \leq 0.005$]. There were no significant differences between LongC and Short at the beginning of movement. Since the pattern of effects for peak acceleration shown in Figure 1B are similar to the pattern for theta band in Domain 1, these results suggest acceleration effects in the theta band at the beginning of movement. This was explored using correlation analysis between ERSP power and acceleration. Indeed we observed a significant positive correlation between theta activity at the beginning of movement and peak acceleration (Table 4). There was also a significant positive relation between ERSP power and peak velocity, but the other kinematic measures were not significant. The mu rhythm is typically described between 9–13 Hz, and there was no clear emergent pattern of mu band activity across task condition.

The LongF condition had greater spectral power than the Short condition and LongC condition in the beta band near the end of movement [t(14)'s≥3.34,p's≤0.005]. Also, LongC had greater spectral power than the Short condition in the beta band near the end of movement [t(14)'s≥3.34,p's≤0.005]. The timing of these beta band changes are occurring when the peak deceleration occurs. When examining the correlation between kinematic parameters and beta activity, we found that only movement time was significantly related to beta activity (Table 4).

Figure 3 A shows a right motor area that is primarily associated with primary, premotor, and supplementary motor cortex (BA 4 and 6) and primary somatosensory cortex (BA 3). Figure 3B shows the time-frequency spectral plots from ERSP Domain 2. Figure 3C shows time-frequency contrast plots that indicate statistical significance between the LongF and Short conditions and the LongF and LongC conditions. Statistical analysis revealed that the LongF condition had lower spectral power than the Short and LongC conditions in the alpha band (or mu band) near the end of the movement [t(14)'s≤-3.34,p's≤0.005]. This pattern in the alpha band near the end of movement was not related to any of the kinematic variables (Table 4). This suggests that alpha band changes in ipsilateral motor areas may be related to parameters other than the kinematics of the movement. Ipsilateral mu band activity was observed during similar time intervals as contralateral beta band activity.

Figure 4A shows ERSP Domain 3, a right somatosensory area. This area is associated with the somatosensory association cortex, secondary and associative visual (BA 18 and 19) areas. Figure 4B shows the time-frequency spectral plots from the right somatosensory area across all conditions. Figure 4C shows the time-frequency spectral contrast plots that compare the LongF vs. Short, LongF vs. LongC, and LongC and Short conditions. The LongF condition had lower spectral power in the alpha and beta band near the end of the movement as compared to both the Short and LongC conditions [t(14)'s≤-3.34,p's≤0.005]. We did not observe similar alpha and beta band changes for the LongC vs. Short comparison. This pattern in the alpha and beta bands in the right somatosensory area near the end of movement was not related to any of the kinematic variables (Table 4).

Figure 5A shows ERSP Domain 4, a visual area, that is associated with the primary (BA 17), secondary, and associative visual cortex and limbic association cortex area (BA 23 and 30). Figure 5B shows the visual area time-frequency spectral plots across conditions. Figure 5C shows the LongF condition had greater spectral power than the Short and LongC condition in the gamma band about two-thirds of the way through the movement [t(14)'s≥3.34,p's≤0.005]. A similar observation was seen for the LongC condition with greater power than the Short condition [t(14)'s≥3.34,p's≤0.005]. The timing is consistent with the deceleration phase of the movement when movement is slowing down the cursor. The gamma band activity was significantly correlated with peak velocity, suggesting that gamma band activity changed according to how fast the movement was occurring.

Source-Space Cortical Dynamics: Inter-trial Coherence

Figure 6A shows the two domains from the ITC analysis, and 6B shows the ITC results within each movement condition. Table 5 shows that ITC Domain 1 covered left premotor and supplementary motor area, primary motor cortex, and primary somatosensory cortex.

ITC Domain 2 covered premotor and supplementary motor area and cingulate cortex (Table 5). Domain 2 is more medial and anterior in its location than Domain 1. Figure 6B shows that there is a clear theta band activity in the Short and LongF conditions, which is less evident in the LongC condition. Figure 6C shows the statistical comparisons for the ITC results. In ITC Domain 1, we found greater ITC near the beginning of movement in the theta band for the LongF vs. Short, LongF vs. LongC [$t(14)$'s$\geq$3.34,p's$\leq$0.005], and Short vs. LongC [$t(14)$'s$\geq$-3.34,p's$\leq$0.005]. In ITC Domain 2, we found greater ITC near the beginning of movement in the theta band for Short vs. LongF, Short vs. LongC [$t(14)$'s$\geq$-3.34,p's$\leq$0.005] and LongF vs. LongC [$t(14)$'s$\geq$3.34,p's$\leq$0.005].

4. Discussion

We investigated how source space cortical dynamics relate to movement kinematics in humans during an upper limb ballistic movement. In the left motor area contralateral to the moving limb, we observed an increase in the amplitude of theta band activity with increased movement acceleration at the beginning of movement. This conclusion was supported by a significant correlation between theta activity and peak acceleration at the beginning of movement. The beta band activity increased during the deceleration phase of the movement, and this was related to movement time and possibly signaled a return to tonic muscle activity (Jenkinson and Brown 2011) or motor slowing (Pogosyan et al., 2009). In the ipsilateral motor and somatosensory areas, the amplitude of alpha band activity decreased during the deceleration phase of movement, but this was not related to movement kinematics. In visual cortex, gamma band activity increased during the deceleration phase of movement, and this was correlated with movement velocity. Our results suggest that humans use distinct lateralized cortical activity for distance and speed dependent arm movements. We provide new evidence that a temporary increase in theta band power relates to movement acceleration and is important during movement execution. Further, the theta power increase is coupled with decreased beta and alpha band power which are modulated by the task near the end of movement.

4.1. The role of theta in movement execution

Theta band activity has been interpreted in the context of sensorimotor integration, with region specific increases in theta activity thought to reflect increases in sensorimotor processing (Bland 1986; Cruikshank et al., 2012). Changes in the visibility of a target stimulus at movement initiation has been associated with changes in theta band activity from temporal electrodes, thought to reflect sensorimotor processes in the ventral visual processing stream. Importantly, the authors reported that theta activity from the Fz electrode (over motor regions) did not differ as a function of task condition, likely because even though the visual stimuli differed across conditions the movements that were made did not (Cruikshank et al., 2012). Here, we demonstrate that theta activity in the contralateral motor cortex is sensitive to movement acceleration when the parameters of a movement task are precisely manipulated. Using ITC analysis, we also determined that phase-locking occurred in the theta band at the beginning of movement in the contralateral motor domains. The ITC also covaried with the type of ballistic movement during the acceleration phase.

Theta oscillations have been observed in raw intracranial signals recorded from humans, and are more frequent during complex tasks (Kahana et al., 1999) and during virtual movements compared to periods of voluntary stillness (Caplan et al., 2003). Exploratory search behavior compared with goal-seeking behaviors exhibit theta oscillations at different cortical sites suggesting that region specific theta oscillations may depend on which regions are involved in a specific kind of behavior, and when that particular region is engaged (Caplan et al., 2003). It is established from single cell recordings in non-human primates that changes in direction and velocity require changes in the activity of pyramidal tract neurons in the motor cortex (Ashe and Georgopoulos 1994). Human neuroimaging work has further demonstrated that the primary motor cortex contralateral to the moving limb plays a critical role in scaling specific parameters of motor function such as amplitude and velocity (Turner et al., 2003). The study by Turner and colleagues did not quantify acceleration. However, when visually examining their velocity data in Figure 2, the velocity fluctuations were greater as the tracking amplitude increased, suggesting that the acceleration was increasing with increased tracking amplitude and velocity. The current study extends the elegant studies by Turner and colleagues since we quantified distance, velocity, acceleration, deceleration and error in relation to source space cortical dynamics.

The findings from the current study suggest that acceleration is a key movement parameter of interest in the motor cortex. We also observed a significant correlation between theta band activity and peak velocity, although the correlation was greater for peak acceleration. The main difference between the prior work in non-human primates is that we have studied humans using source space cortical oscillations and examined the relation with specific parameters of the movement time course (e.g., peak acceleration), whereas the influential work of Ashe and Georgopoulus studied the whole time course and regressed the parameters against single cell discharge recordings in non-human primates. Furthermore, single-cell recordings reflect spiking of neurons that have high frequency signals, whereas local field potentials have lower frequencies and are mostly due to synaptic activity averaged across a region of brain tissue. It should be noted that some reports suggest that scalp recordings are more precise measures of neural processes that regulate behavior than single unit recordings (Mehring et al., 2003; Scherberger et al., 2005). Our findings add to the literature that the motor cortex contains substantial information about upper arm movements and modulates theta oscillations for sensorimotor processing. Theta phase synchrony is thought to be an important mechanism in the integration of neural ensembles. Theta band activity is thought to have an important role in facilitation of sensory and cognitive performance in animals and humans. Some authors suggest that these long-range binding mechanisms are also engaged during regulatory top-down control (Engel et al., 2001, Canolty and Knight, 2010 and Sauseng et al., 2010). We found increased theta phase coherence and power in the contralateral motor cortex. In line with these findings, theta power from the motor cortex could function as a signature for enhanced control engagement across cortical domains.

Our observations suggest that theta band activity is associated with adaptive adjustments required for the ongoing regulation of upper limb movements. Indeed, variations in theta oscillations may reflect neural mechanisms that allocate cognitive resources (Sauseng et al., 2007). We also found that theta synchrony was located in premotor cortices and anterior cingulate cortex, and was likely related to the observed amplitude differences of theta at the

beginning of movement. It has been proposed that theta synchronization in anterior cingulate cortex is central for motor execution and higher order control areas (Paus, 2001). Taken together it is clear that theta band power is related to the current upper limb movement task, and in particular the acceleration of the movement.

4.2. The role of alpha, beta, and gamma in movement cessation

Movement-related beta oscillations over bilateral motor cortex exhibit a sharp decrease in spectral power at the beginning of movement (Cruikshank et al., 2012; Gwin and Ferris 2012; Kilavik et al., 2013; Pastotter et al., 2012). In the current study, we did observe this classic bilateral reduction in beta band activity, with greater reductions evidenced in the contralateral hemisphere. In the contralateral motor area, beta band activity did not change with movement acceleration at the beginning of movement, but did increase with the task condition during the deceleration phase of the movement. Beta band activity preceding a choice-reaction time task has been shown to vary as participants focus on accelerating the limb rather than accuracy (Pastotter et al., 2012). Pastotter and colleagues did not find any changes in peak beta band power after the beginning of movement. Our findings extend this work and suggest there are differences in beta band activity near the end of the movement. It is also the case that the triceps EMG was different in phases 3 and 4 of the movement, when the beta band was changing in the contralateral motor area. The only kinematic parameter that was related to the beta band activity during the deceleration phase of the movement was movement time. These findings are consistent with the interpretation that beta band activity could be signaling a return to the tonic state or motor slowing (Jenkinson and Brown 2011; Pogosyan et al., 2009).

In their review paper, Jenkinson and Brown (2010) based their hypothesis that beta activity promotes tonic activity on considerable data from individuals with Parkinson’s disease off and on medication and during neurosurgery (Kühn et al., 2006; Ray et al., 2008). In the current paper, all three conditions had reduced beta-band activity during movement, but the LongF condition evidenced increased beta-activity compared with the other slower conditions. Since this difference occurred during the deceleration phase of movement and correlated with movement time, our findings are consistent with the hypothesis that beta band activity could aid in motor slowing and processes that may aid the movement in returning to a tonic state. Further, Pogosyan and colleagues (2009) demonstrate a causal slowing in voluntary movement using sinusoidal transcranial alternating-current stimulation at 20Hz. Our current data are also consistent with this hypothesis given that during the deceleration phase the subject is slowing down the limb to arrive at the stationary target.

The amplitude of alpha band activity decreases during movement, and this is consistent with the interpretation of event-related desynchronization (Babiloni et al., 1999; Toro et al., 1994), which is thought to reflect the excitability of neurons and hence reflect activation in a specific cortical area (Neuper and Pfurtscheller 2001). We observed reduced alpha band activity near the end of movement in the ipsilateral motor and somatosensory regions. This pattern of findings for the alpha band was not correlated with a specific movement kinematic parameter. A recent study by Tan and colleagues indicate that trial to trial adaptation in movement error relates to the beta band activity several hundred milliseconds

post movement (Tan et al., 2014). The authors also observed effects in the alpha band post movement, but this frequency band was mostly related to the trial duration.

Recent theoretical models for alpha oscillations suggest that alpha event-related synchronization reflects inhibition, and a decrease in the amplitude of alpha band activity reflects a release from inhibition (Klimesch 2012). Our findings support this view, since alpha band power decreased during the movement. Klimesh argues for a specific role of alpha band activity in modulating attention across networks. Stimulating the ipsilateral motor cortex reduces the excitability of the contralateral motor cortex and this is termed interhemispheric inhibition (Avanzino et al., 2007; Ferbert et al., 1992). In the current experiment, we observed that the amount of event-related desychronization in alpha band power in the ipsilateral motor and somatosensory regions varied with the task demands near the end of movement but did not relate to a kinematic parameter. After peak velocity, subjects decelerated their movements to ensure that the cursor would land in the target region and the triceps EMG activity covaried with the task in phases 3 and 4. Prior to cessation of a movement, inhibitory circuits are elevated and are thought to play a role in slowing the movement (Buccolieri et al., 2004; Toma et al., 1999). Since alpha-band activity was further suppressed in the LongF condition compared with the other two conditions, our findings are supportive of this interpretation. It is important to also note that mu band activity is typically suppressed during movement execution (Pfurtscheller et al., 1994) and we observed this same type of suppression using the ERSP analysis approach.

Deceleration related gamma band activity was found in the right visual area about two-thirds of the way through the movement. This finding is consistent with observations of increased gamma band activity in visual areas when monkeys attend to fast changing stimuli (Frien and Eckhorn 2000). Gamma oscillations in the macaque visual cortex have been linked to attentional modulation (Ray and Maunsell 2011). Furthermore, several studies have shown an increase in gamma band activity after movement execution in a variety of cortical areas (Ball et al., 2008; Pfurtscheller et al., 1994). In the current study, participants moved as fast as possible to two distances with the LongF condition requiring the fastest acceleration and deceleration. Increased gamma activity in the LongF condition may suggest that fast movements require greater visual processes as the participants attend to the cursor during the deceleration phase, and the visual cortex activity may scale with movement parameters, such as deceleration, during the movement. Our findings suggest that visual cortices play an active role in movement control through power increases in gamma band activity.

5. Conclusion

The findings from this study suggest that electrocortical activity for upper arm movements involves the regulation of a broadband network of oscillations across the cortex throughout movement. Theta band activity changed in the left premotor and motor cortices in relation to movement acceleration. This theta activity was consistent with phase-locked activity because the ITC findings converged with this cortical domain in the theta band. This provides new evidence that theta activity may be facilitating control strategies for the ballistic phase of the movement. Increased beta band activity in contralateral motor areas occurred during the deceleration phase of movement, and may be signaling a return to tonic

muscle activity. Alpha band activity decreases were evidenced during movement in ipsilateral motor and somatosensory areas, but the amount of event-related spectral activity in the alpha band was not related to specific kinematic parameters of movement. Finally, gamma band oscillations from the visual cortex may be related to attending to the fast changing visual stimulus during movement control. These findings, which were developed in the context of a 3D cortical electrophysiology paradigm in humans, provide a novel approach to explore the cortical dynamics of ballistic limb movements in a variety of movement disorders and stroke.

Acknowledgment

This work was supported by NINDS R01 NS058487 and R01 NS052318. The authors declare no competing financial interests

References

Allen DP, MacKinnon CD. Time-frequency analysis of movement-related spectral power in EEG during repetitive movements: a comparison of methods. J Neurosci Methods. 2010; 186(1):107–115. [PubMed: 19909774]

Ashe J, Georgopoulos AP. Movement parameters and neural activity in motor cortex and area 5. Cereb Cortex. 1994; 4(6):590–600. [PubMed: 7703686]

Avanzino L, Teo JT, Rothwell JC. Intracortical circuits modulate transcallosal inhibition in humans. J Physiol. 2007; 583(Pt 1):99–114. [PubMed: 17556392]

Babiloni C, Carducci F, Cincotti F, Rossini PM, Neuper C, Pfurtscheller G, Babiloni F. Human movement-related potentials vs desynchronization of EEG alpha rhythm: a high-resolution EEG study. Neuroimage. 1999; 10(6):658–665. [PubMed: 10600411]

Ball T, Demandt E, Mutschler I, Neitzel E, Mehring C, Vogt K, Aertsen A, Schulze-Bonhage A. Movement related activity in the high gamma range of the human EEG. Neuroimage. 2008; 41(2): 302–310. [PubMed: 18424182]

Bigdely-Shamlo N, Mullen T, Kreutz-Delgado K, Makeig S. Measure projection analysis: a probabilistic approach to EEG source comparison and multi-subject inference. Neuroimage. 2013; 72:287–303. [PubMed: 23370059]

Bland BH. The physiology and pharmacology of hippocampal formation theta rhythms. Prog Neurobiol. 1986; 26(1):1–54. [PubMed: 2870537]

Bollimunta A, Chen Y, Schroeder CE, Ding M. Neuronal mechanisms of cortical alpha oscillations in awake-behaving macaques. J Neurosci. 2008; 28(40):9976–9988. [PubMed: 18829955]

Buccolieri A, Abbruzzese G, Rothwell JC. Relaxation from a voluntary contraction is preceded by increased excitability of motor cortical inhibitory circuits. J Physiol. 2004; 558(Pt 2):685–695. [PubMed: 15181164]

Caplan JB, Madsen JR, Schulze-Bonhage A, Aschenbrenner-Scheibe R, Newman EL, Kahana MJ. Human theta oscillations related to sensorimotor integration and spatial learning. J Neurosci. 2003; 23(11):4726–4736. [PubMed: 12805312]

Cruikshank LC, Singhal A, Hueppelsheuser M, Caplan JB. Theta oscillations reflect a putative neural mechanism for human sensorimotor integration. J Neurophysiol. 2012; 107(1):65–77. [PubMed: 21975453]

Delorme A, Makeig S. EEGLAB: an open source toolbox for analysis of single-trial EEG dynamics including independent component analysis. J Neurosci Methods. 2004; 134(1):9–21. [PubMed: 15102499]

Ferbert A, Priori A, Rothwell JC, Day BL, Colebatch JG, Marsden CD. Interhemispheric inhibition of the human motor cortex. J Physiol. 1992; 453:525–546. [PubMed: 1464843]

Frien A, Eckhorn R. Functional coupling shows stronger stimulus dependency for fast oscillations than for low-frequency components in striate cortex of awake monkey. Eur J Neurosci. 2000; 12(4): 1466–1478. [PubMed: 10762374]

Gwin JT, Ferris DP. An EEG-based study of discrete isometric and isotonic human lower limb muscle contractions. J Neuroeng Rehabil. 2012; 9:35. [PubMed: 22682644]

Gwin JT, Gramann K, Makeig S, Ferris DP. Removal of movement artifact from high-density EEG recorded during walking and running. J Neurophysiol. 2010; 103(6):3526–3534. [PubMed: 20410364]

Jenkinson N, Brown P. New insights into the relationship between dopamine, beta oscillations and motor function. Trends in Neurosciences. 2011; 34(12):611–618. [PubMed: 22018805]

Jurkiewicz MT, Gaetz WC, Bostan AC, Cheyne D. Post-movement beta rebound is generated in motor cortex: evidence from neuromagnetic recordings. Neuroimage. 2006; 32(3):1281–1289. [PubMed: 16863693]

Kahana MJ, Sekuler R, Caplan JB, Kirschen M, Madsen JR. Human theta oscillations exhibit task dependence during virtual maze navigation. Nature. 1999; 399(6738):781–784. [PubMed: 10391243]

Kilavik BE, Zaepffel M, Brovelli A, MacKay WA, Riehle A. The ups and downs of beta oscillations in sensorimotor cortex. Exp Neurol. 2013; 245:15–26. [PubMed: 23022918]

Klimesch W. alpha-band oscillations, attention, and controlled access to stored information. Trends Cogn Sci. 2012; 16(12):606–617. [PubMed: 23141428]

Kühn AA, Kupsch A, Schneider G-H, Brown P. Reduction in subthalamic 8–35 Hz oscillatory activity correlates with clinical improvement in Parkinson's disease. European Journal of Neuroscience. 2006; 23(7):1956–1960. [PubMed: 16623853]

Lopes da Silva FH, Vos JE, Mooibroek J, Van Rotterdam A. Relative contributions of intracortical and thalamo-cortical processes in the generation of alpha rhythms, revealed by partial coherence analysis. Electroencephalogr Clin Neurophysiol. 1980; 50(5–6):449–456. [PubMed: 6160987]

McFarland DJ, Miner LA, Vaughan TM, Wolpaw JR. Mu and beta rhythm topographies during motor imagery and actual movements. Brain Topogr. 2000; 12(3):177–186. [PubMed: 10791681]

Mehring C, Rickert J, Vaadia E, de Oliveira SC, Aertsen A, Rotter S. Inference of hand movements from local field potentials in monkey motor cortex. Nat Neurosci. 2003; 6(12):1253–1254. [PubMed: 14634657]

Neuper C, Pfurtscheller G. Event-related dynamics of cortical rhythms: frequency-specific features and functional correlates. Int J Psychophysiol. 2001; 43(1):41–58. [PubMed: 11742684]

Pastotter B, Berchtold F, Bauml KH. Oscillatory correlates of controlled speed-accuracy tradeoff in a response-conflict task. Hum Brain Mapp. 2012; 33(8):1834–1849. [PubMed: 21618665]

Pfurtscheller G, Flotzinger D, Neuper C. Differentiation between finger, toe and tongue movement in man based on 40 Hz EEG. Electroencephalogr Clin Neurophysiol. 1994; 90(6):456–460. [PubMed: 7515789]

Pfurtscheller G, Neuper C. Event-related synchronization of mu rhythm in the EEG over the cortical hand area in man. Neurosci Lett. 1994; 174(1):93–96. [PubMed: 7970165]

Pogosyan A, Gaynor LD, Eusebio A, Brown P. Boosting Cortical Activity at Beta-Band Frequencies Slows Movement in Humans. Current Biology. 2009; 19(19):1637–1641. [PubMed: 19800236]

Ray NJ, Jenkinson N, Wang S, Holland P, Brittain JS, Joint C, Stein JF, Aziz T. Local field potential beta activity in the subthalamic nucleus of patients with Parkinson's disease is associated with improvements in bradykinesia after dopamine and deep brain stimulation. Experimental Neurology. 2008; 213(1):108–113. [PubMed: 18619592]

Ray S, Maunsell JH. Different origins of gamma rhythm and high-gamma activity in macaque visual cortex. PLoS Biol. 2011; 9(4):e1000610. [PubMed: 21532743]

Salmelin R, Hari R. Spatiotemporal characteristics of sensorimotor neuromagnetic rhythms related to thumb movement. Neuroscience. 1994; 60(2):537–550. [PubMed: 8072694]

Scherberger H, Jarvis MR, Andersen RA. Cortical Local Field Potential Encodes Movement Intentions in the Posterior Parietal Cortex. Neuron. 2005; 46(2):347–354. [PubMed: 15848811]

Shattuck DW, Chiang MC, Barysheva M, McMahon KL, de Zubicaray GI, Meredith M, Wright MJ, Toga AW, Thompson PM. Visualization tools for high angular resolution diffusion imaging. Med Image Comput Comput Assist Interv. 2008; 11(Pt 2):298–305. [PubMed: 18982618]

Tan H, Jenkinson N, Brown P. Dynamic Neural Correlates of Motor Error Monitoring and Adaptation during Trial-to-Trial Learning. The Journal of Neuroscience. 2014; 34(16):5678–5688. [PubMed: 24741058]

Toma K, Honda M, Hanakawa T, Okada T, Fukuyama H, Ikeda A, Nishizawa S, Konishi J, Shibasaki H. Activities of the primary and supplementary motor areas increase in preparation and execution of voluntary muscle relaxation: an event-related fMRI study. J Neurosci. 1999; 19(9):3527–3534. [PubMed: 10212312]

Toro C, Cox C, Friehs G, Ojakangas C, Maxwell R, Gates JR, Gumnit RJ, Ebner TJ. 8–12 Hz rhythmic oscillations in human motor cortex during two-dimensional arm movements: evidence for representation of kinematic parameters. Electroencephalogr Clin Neurophysiol. 1994; 93(5): 390–403. [PubMed: 7525247]

Turner RS, Desmurget M, Grethe J, Crutcher MD, Grafton ST. Motor subcircuits mediating the control of movement extent and speed. J Neurophysiol. 2003; 90(6):3958–3966. [PubMed: 12954606]

Vaillancourt DE, Prodoehl J, Verhagen Metman L, Bakay RA, Corcos DM. Effects of deep brain stimulation and medication on bradykinesia and muscle activation in Parkinson's disease. Brain. 2004; 127(Pt 3):491–504. [PubMed: 14662520]

Highlights

- We use Measure Projection Analysis for source dynamics in upper arm movements
- We show 3D maps with statistical significance for ERSP and ITC measures in upper limb movements
- We propose that theta activity from premotor and the contralateral motor cortex is involved in movement execution, particularly movement acceleration
- We found that distinct lateralized cortical activity is recruited at the end of movement

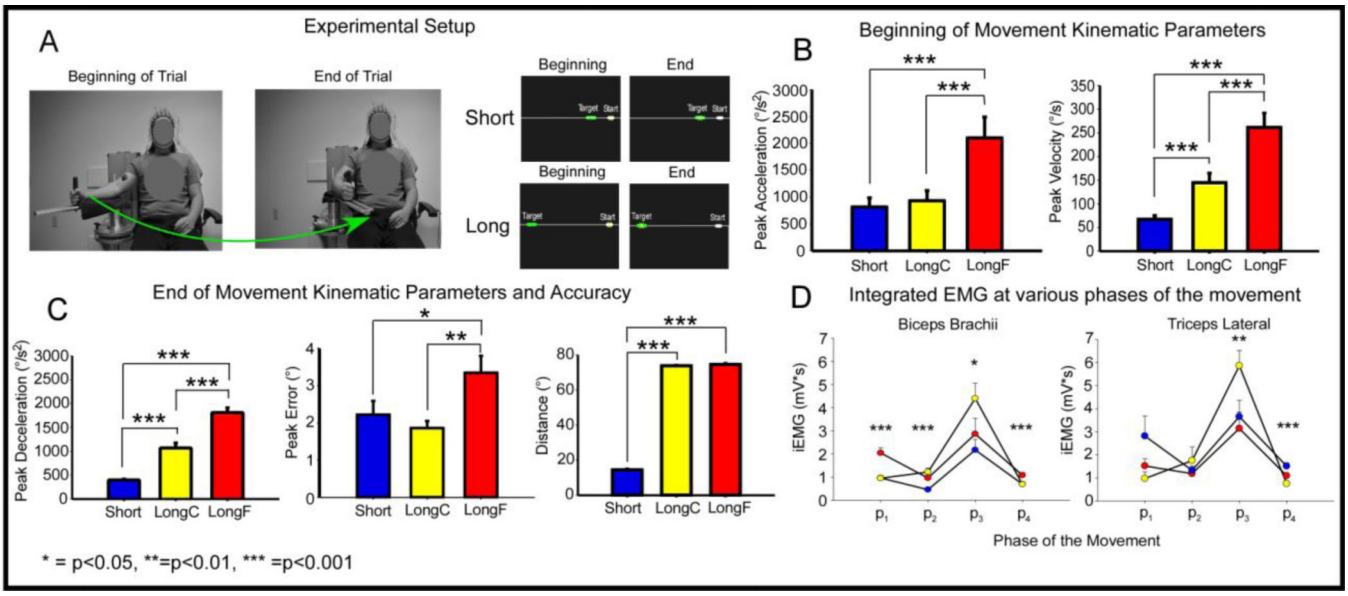

Figure 1.

Experimental Setup and Kinematic and EMG results. Figure 1A shows a participant with their right arm attached to the manipulandum in the start and end position. The participant is wearing EEG and EMG electrodes. Figure 1A also shows the visual display from the computer monitor at the beginning and end of the task for the Short and Long condition. The white cursor indicates the start position, the green cursor indicates the target position, and the yellow cursor indicates the actual position of the participant. Figure 1B shows bar graphs of peak acceleration and peak velocity during the initial phase of movement for the Short, LongC, and LongF conditions with positive standard error bars. Figure 1C shows bar graphs with positive standard error bars of peak deceleration, peak error, and distance for the Short, LongC, and LongF conditions. Figure 1D left panel shows multiple line plots of the average EMG profile (averaged across all trials and subjects per condition) for the biceps brachii and triceps lateral across conditions. The vertical dashed lines are average peak acceleration, average peak velocity, and average peak deceleration. Figure 1D right panel shows scatter-line plots with positive standard error bars of integrated EMG data for the biceps brachii and triceps lateral at four phases of movement across the Short, LongF, and LongC condition. The x-axis denotes the 4 phases of movement with p_1 representing the beginning of movement to peak acceleration, p_2 peak acceleration to peak velocity, p_3 peak velocity to peak deceleration and p_4 peak deceleration to the end of the movement.

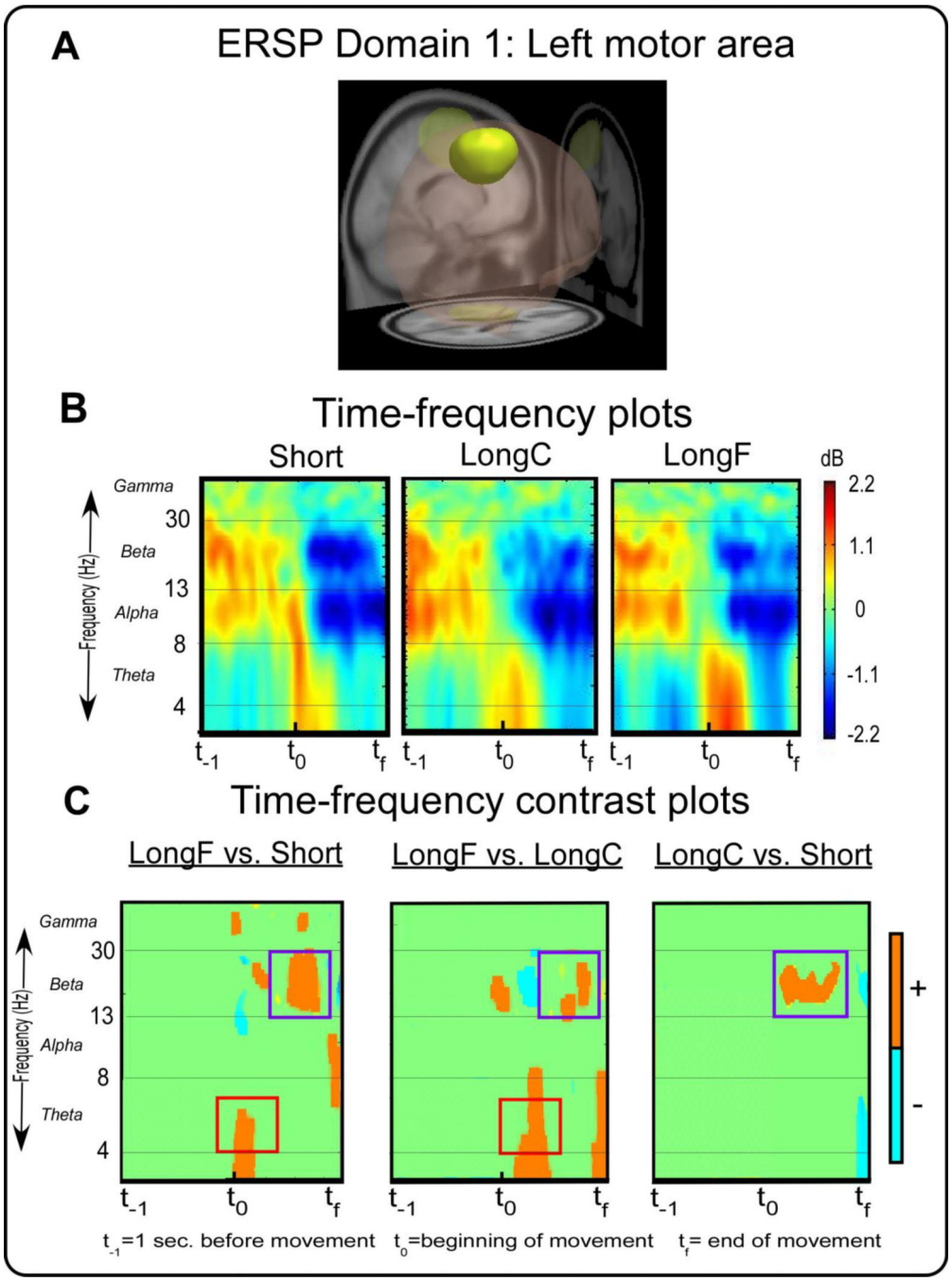

Figure 2.

ERSP measure domain 1 and time-frequency spectral plots. Figure 2A displays a 3D representation of the brain area. The yellow region indicates the domain revealed by MPA , the left motor area. Figure 2B displays time-frequency spectral plots of the Short, LongC, and LongF conditions. The x-axis denotes time with t_{-1} representing one second prior to movement onset, t_0 movement onset, and t_f the end of the movement. The y-axis depicts log frequency 0 to 50 with the major EEG bands, theta, alpha, beta, and gamma labeled. The plots are color scaled based on decibel where positive values are warm colors and negative

values are cool colors. Figure 2C displays time-frequency contrast statistical plots of the LongF vs. Short, LongF vs. LongC, and LongC vs. Short conditions. Orange indicates positive significant test values of the statistical contrast plot whereas blue indicates negative significant test values of the statistical contrast, green indicates non-significant areas of the plots. The open-red squares and open-purple squares highlight effects that are consistent with the pattern of acceleration and deceleration, respectively.

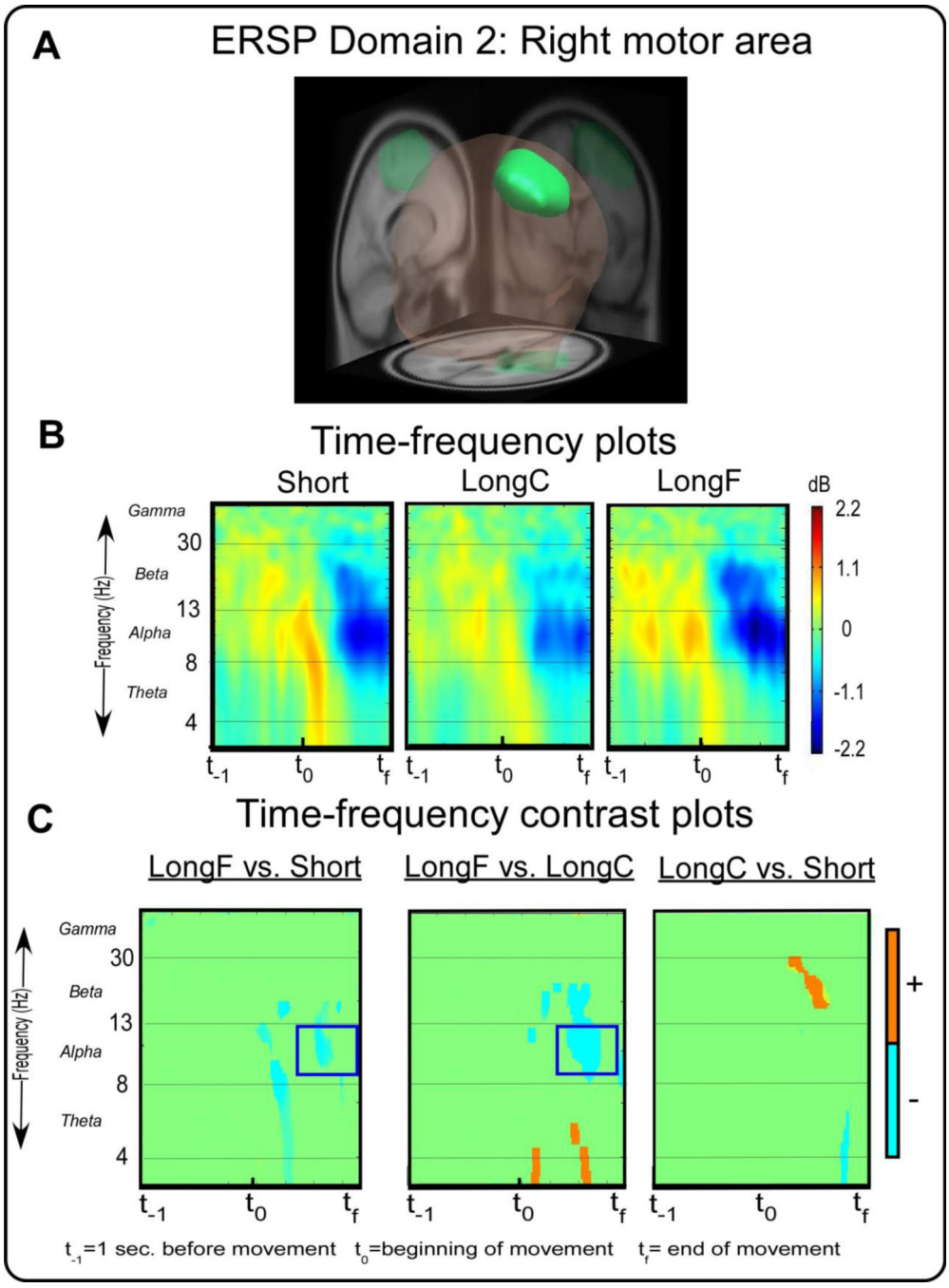

Figure 3.

ERSP measure domain 2 and time-frequency spectral plots. Figure 3A displays a 3D46representation of the brain area. The green region indicates the domain revealed by MPA, the right motor area. Figure 3B displays time-frequency spectral plots of the Short, LongC, and LongF conditions. The x-axis denotes time with t_{-1} representing one second prior to movement onset, t_0 movement onset and t_f the end of the movement. The y-axis depicts log frequency 0 to 50 with the major EEG bands, theta, alpha, beta, and gamma labeled. The plots are color scaled based on decibel where positive values are warm colors

and negative values are cool colors. Figure 3C displays time-frequency contrast statistical plots of the LongF vs. Short, LongF vs. LongC, and LongC vs. Short conditions. Orange indicates positive significant test values of the statistical contrast plot whereas blue indicates negative significant test values of the statistical contrast, green indicates non-significant areas of the plots. The open-blue squares highlight effects that are consistent with the pattern of movement error.

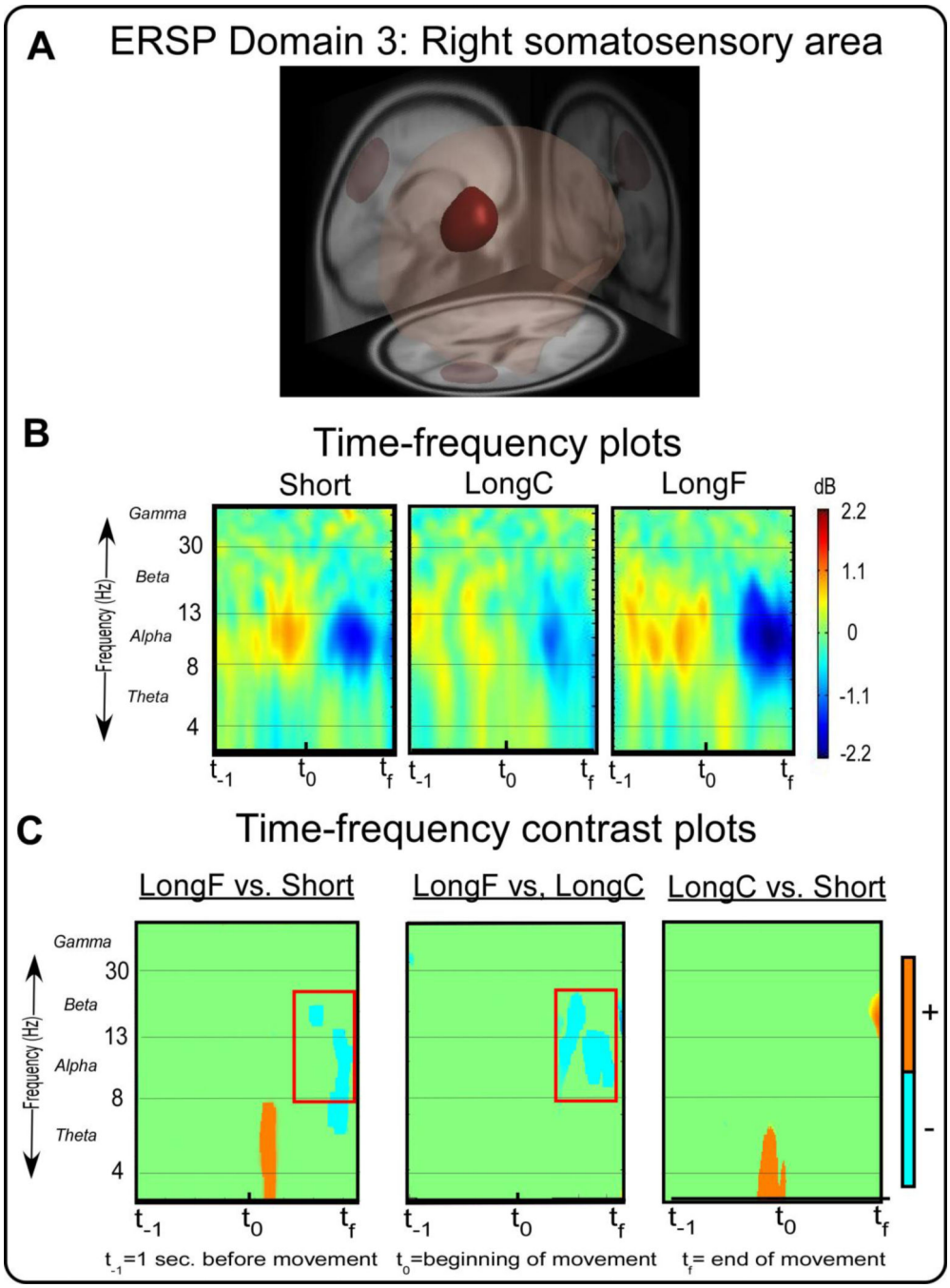

Figure 4.

ERSP measure domain 3 and time-frequency plots. Figure 4A displays a 3D representation of the brain area. The maroon region indicates the domain revealed by MPA, the right somatosensory motor area. Figure 4B displays time-frequency spectral plots of the Short, LongC, and LongF conditions. The x-axis denotes time with t_{-1} representing one second prior to movement onset, t_0 movement onset, and t_f the end of the movement. The y-axis depicts log frequency 0 to 50 with the major EEG bands, theta, alpha, beta, and gamma labeled. The plots are color scaled based on decibel where positive values are warm colors

and negative values are cool colors. Figure 4C displays time-frequency contrast statistical plots of the LongF vs. Short, LongF vs. LongC, and LongC vs. Short conditions. Orange indicates positive significant test values of the statistical contrast plot whereas blue indicates negative significant test values of the statistical contrast, green indicates non-significant areas of the plots. The open-blue squares highlight effects that are consistent with the pattern of movement error.

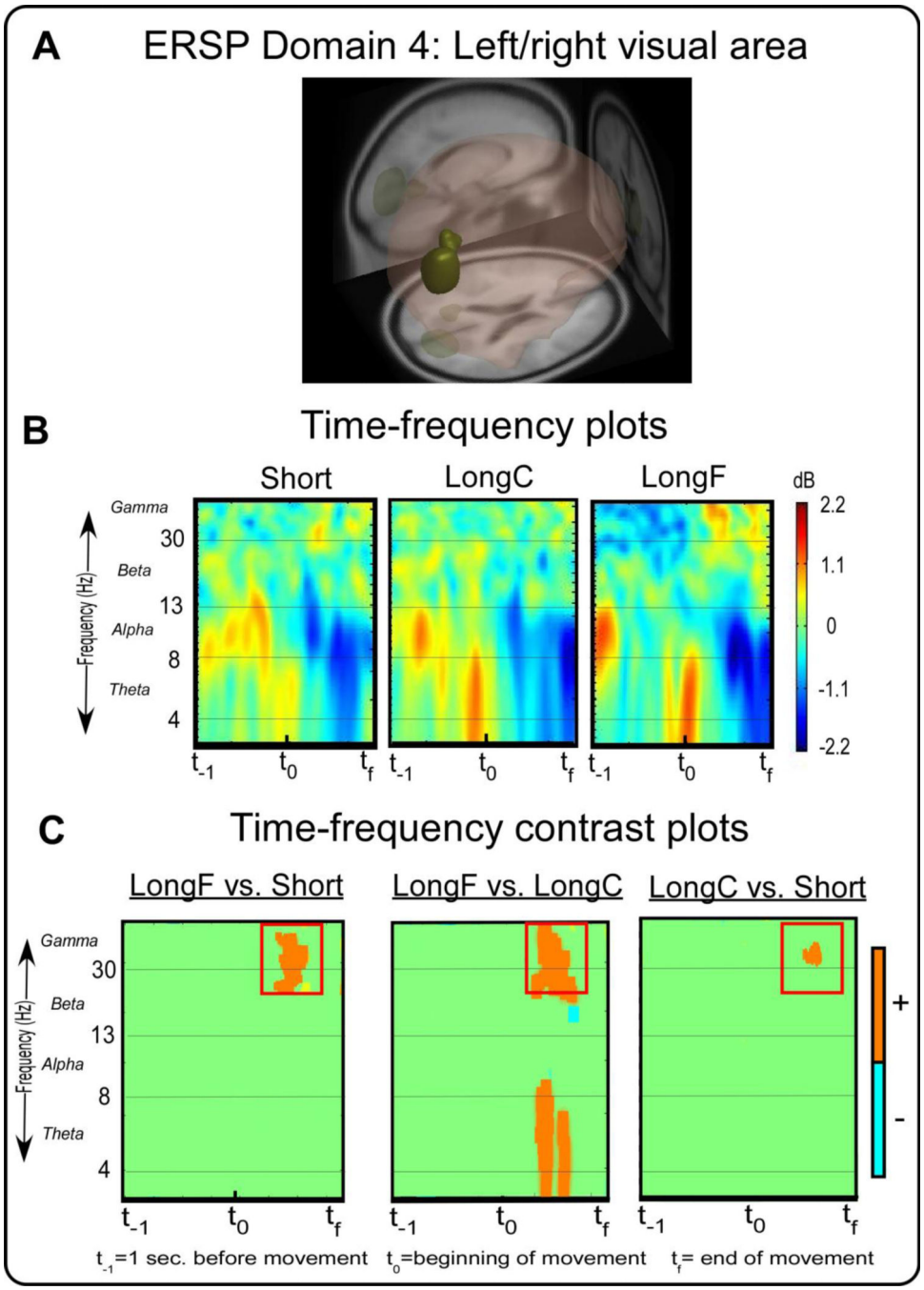

Figure 5.

ERSP measure domain 4 and time-frequency spectral plots. Figure 5A displays a 3D representation of the brain area. The dark yellow-green region indicates the domain revealed by MPA, the right visual motor area. Figure 5B displays time-frequency spectral plots of the Short, LongC, and LongF conditions. The x-axis denotes time with t_{-1} representing one second prior to movement onset, t_0 movement onset, and t_f the end of the movement. The y-axis depicts log frequency 0 to 50 with the major EEG bands, theta, alpha, beta, and gamma labeled. The plots are color scaled based on decibel where positive values are warm colors

and negative values are cool colors. Figure 5C displays time-frequency contrast statistical plots of the LongF vs. Short, LongF vs. LongC, and LongC vs. Short conditions. Orange indicates positive significant test values of the statistical contrast plot whereas blue indicates negative significant test values of the statistical contrast. The open-purple squares highlight effects that are consistent with the pattern of movement error.

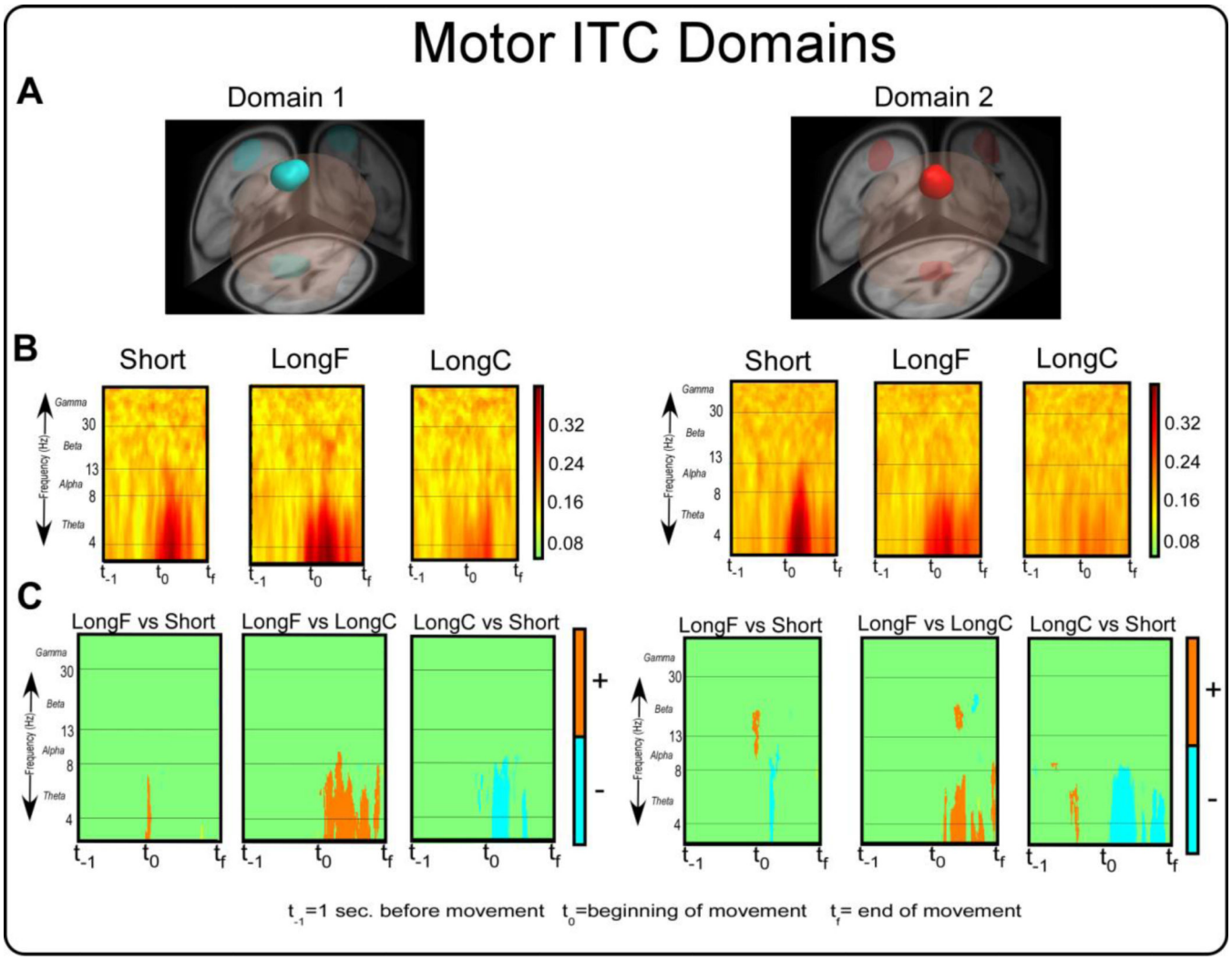

Figure 6.

ITC measure domains 1 and 2 and their corresponding time-frequency spectral plots. Figure 6A displays 3D representations of the brain areas. The light blue and bright red areas indicate the domains revealed by MPA. Figure 6B displays time-frequency spectral plots of the Short, LongC, and LongF conditions. The x-axis denotes time with t_{-1} representing one second prior to movement onset, t_0 movement onset, and t_f the end of the movement. The y-axis depicts log frequency 0 to 50 with the major EEG bands, theta, alpha, beta, and gamma labeled. The plots are color scaled based on coherence where higher values are dark warm colors and low values are light warm colors. Figure 6C displays time-frequency contrast statistical plots of the LongF vs. Short, LongF vs. LongC, and LongC vs. Short conditions. Orange indicates positive significant test values of the statistical contrast plot whereas blue indicates negative significant test values of the statistical contrast.

Table 1

Behavioral mean values and Bonferonni pairwise comparisons for each condition

	Short (mn,SE)	LongC (mn,SE)	LongF (mn,SE)	Repeated measures Anova statistic and p-value	Pairwise comparison p-values
Peak Acceleration (°/s^2)	815.4 (169.7)	932.3 (188.9)	2100.3 (387.6)	F(2,28)=17.3,p<0.001	A<0.001; B<0.001; C=0.99
Peak Velocity (°/s)	69.4 (7.0)	150.7 (18.4)	275.4 (28.6)	F(2,28)=67.2,p<0.001	A<0.001; B<0.001; C<0.001
Peak Deceleration (°/s^2)	398.6 (17.1)	1069.1 (104.4)	1810.6 (99.4)	F(2,28)=76.6,p<0.001	A<0.001; B<0.001; C<0.001
Movement Time (ms)	646.0 (21.1)	1031.6 (64.3)	806.5 (69.0)	F(2,28)=16.2,p<0.001	A=0.11; B<0.05; C<0.01
Peak Error (°)	2.2 (0.4)	1.8 (0.2)	3.3 (0.4)	F(2,28)=9.62,p<0.001	A<0.01; B<0.05; C=0.75
Distance (°)	14.2 (0.4)	73.8 (0.2)	74.3 (0.2)	F(2,28)=14339,p<0.001	A=0.75; B<0.001; C<0.001

A=LongC vs. LongF; B=LongF vs. Short; C=LongC vs. Short

Table 2

A. Integrated EMG mean values for biceps brachii and Bonferroni pairwise comparisons

	Short (mn,SE)	LongC (mn,SE)	LongF (mn,SE)	Repeated measures Anova statistic and p-value	Pairwise comparison p-values
Phase 1	0.96 (0.09)	0.95 (0.11)	2.04 (0.22)	F(2,28)=23.7,p<0.001	A<0.001; B<0.001; C=0.99
Phase 2	0.46 (0.02)	1.22 (0.17)	0.96 (0.11)	F(2,28)=11.4,p<0.001	A=0.62; B<0.002; C<0.001
Phase 3	2.18 (0.46)	4.40 (0.66)	2.87 (0.68)	F(2,28)=6.3,p<0.001	A=0.09; B=0.56; C<0.05
Phase 4	0.70 (0.08)	0.69 (0.08)	1.08 (0.12)	F(2,28)=19.0, p<0.001	A<0.004; B<0.001; C=0.99

B. Integrated EMG mean values for triceps lateral and Bonferroni pairwise comparisons

	Short (mn,SE)	LongC (mn,SE)	LongF (mn,SE)	Repeated measures Anova statistic and p-value	Pairwise comparison p-values
Phase 1	2.82 (0.88)	0.97 (0.30)	1.52 (0.31)	F(2,28)=3.4,p=0.10	A=0.23; B=0.39; C=0.06
Phase 2	1.32 (0.13)	1.75 (0.59)	1.18 (0.34)	[F(2,28)=0.8,p=0.46	A=0.99; B=0.99; C=0.18
Phase 3	3.65 (0.71)	5.52 (0.68)	2.94 (0.71)	F(2,28)=11.0,p=0.002	A<0.05; B=0.09; C<0.01
Phase 4	1.51 (0.15)	0.74 (0.05)	1.09 (0.10)	F(2,28)=13.7, p<0.001	A=0.08; B<0.01; C<0.001

A=LongC vs. LongF; B=LongF vs. Short; C=LongC vs. Short

Table 3

Brodmann and anatomical areas associated with each ERSP domain

ERSP domain	Anatomical area(s)	Brodmann area(s)
1	L Precentral Gyrus (0.37)	**BA 6 (0.48) Premotor and Supplementary Motor**
	L Superior Frontal Gyrus (0.37)	**BA 4 (0.21) Primary Motor**
	L Middle Frontal Gyrus (0.18)	BA 3 (0.17) Primary Somatosenory
	L Postcentral Gyrus (0.08)	BA 31 (0.06)
2	R Precentral Gyrus (0.35)	**BA 6 (0.47) Premotor and Supplementary Motor**
	R Superior Frontal Gyrus (0.35)	**BA 4 (0.21) Primary Motor**
	R Middle Frontal Gyrus (0.16)	BA 3 (0.17) Primary Somatosensory
3	R Superior Parietal Gyrus (0.57)	**BA 7 (0.52) Somatosensory Association**
	R Superior Occipital Gyrus (0.18)	BA 31 (0.19)
	R Angular Gyrus (0.17)	BA 19 (0.16) Associative visual (V3)
	R Middle Occipital Gyrus(0.08)	BA 18 (0.08) Secondary visual (V2)
		BA 39 (0.05)
4	R Lingual Gyrus (0.49)	**BA 18 (0.37) Secondary visual (V2)**
	L Lingual Gyrus (0.21)	BA 30 (0.16)
	R Cuneus (0.10)	BA 19 (0.13) Associative visual (V3)
	R Superior Occipital Gyrus (0.09)	BA 23 (0.13)
	R Middle Occipital Gyrus (0.06)	BA 17 (0.11) Primary visual

Text in bold emphasis shows Brodmann areas (probability > 0.2) most likely assocciated with each domain.

Table 4

Correlation analysis betweeen ERSP power and movement kinematics

	Theta_LMA	Beta_LMA	Alpha_Soma	Alpha_RMA	Gamma_Vis
Peak Acceleration	**r=0.50,p=0.01****	r=0.10,p=0.69	r=−0.23,p=0.29	r=−0.17,p=0.40	r=−0.24,p=0.29
Peak Deceleration	r=−0.18,p=0.41	r=−0.20,p=0.36	r=−0.10,p=0.68	r=0.27,p=0.24	r=−0.33,p=0.12
Peak Velocity	**r=0.41,p=0.04***	r=−0.20,p=0.38	r=−0.33,p=0.12	r=−0.25,p=0.29	**r=0.46,p=0.03***
Movement Time	r=−0.25,p=0.29	**r=−0.40,p=0.04***	r=0.05,p=0.82	r=0.08,p=0.69	r=−0.10,p=0.68
Peak Error	r=−0.15,p=0.48	r=0.22,p=0.28	r=−0.06,p=0.81	r=−0.01,p=0.96	r=−0.04,p=0.84
Distance	r=−0.16,p=0.49	r=−0.17,p=0.32	r=0.03,p=0.84	r=0.09,p-0.72	r=−0.30,p=−0.13

* p<0.05

** p<0.01

LMA=Left Motor Area, RMA=Right Motor Area, Soma=Somatosensory area, Vis=Right/Left Visual area

Table 5

Brodmann and anatomical areas associated with each ITC domain

ITC domain	Anatomical area(s)	Brodmann area(s)
1	L Precentral Gyrus (0.46)	**BA 6 (0.57) Premotor and Supplementary Motor**
	L Superior Frontal Gyrus (0.30)	BA 4 (0.24) Primary Motor
	L Middle Frontal Gyrus (0.20)	BA 3 (0.1 7) Primary Somatosensory
2	L Superior Frontal Gyrus (0.76)	**BA 6 (0.33) Premotor and Supplementary Motor**
	L Cingulate Gyrus (0.14)	**BA 24 (0.32)**
		BA 31 (0.29)
		BA 32 (0.05)

Text in bold emphasis shows Brodmann areas (probability > 0.3) most likely assocciated with each domain.